Journal of Nanoparticle Research (2020) 22: 360
https://doi.org/10.1007/s11051-020-05076-2

RESEARCH PAPER

Microstructure and paramagnetic Meissner effect of $YBa_2Cu_3O_y$ nanowire networks

A. L. Pessoa · A. Koblischka-Veneva · C. L. Carvalho · R. Zadorosny · M. R. Koblischka

Received: 11 May 2020 / Accepted: 29 October 2020 / Published online: 26 November 2020

Abstract The microstructure and magnetic characterizations of non-woven, fabric-like $YBa_2Cu_3O_y$ (YBCO) nanofiber mats are reported. The samples were produced by solution blow spinning (SBS), starting from a sol-gel solution of the precursor materials in polyvinylpyrrolidone. In the present work, the nanowire network samples were morphologically characterized by scanning electron microscopy, and the superconducting properties were measured by magnetometry. An interesting feature is the appearance of a paramagnetic Meissner effect (PME) when field-cooling, firstly verified in that sort of sample. The PME appears only in very small applied magnetic fields, which is similar to previous observations of the PME on an artificially granular YBCO thin film, but distinctly different from bulk samples investigated in the literature. Thus, we explain the PME by flux trapping within the voids of the nanoporous structure of the nanofiber mats.

Keywords Paramagnetic Meissner effect · Solution blow spinning · YBCO nanofiber mats

A. L. Pessoa · C. L. Cavalho · R. Zadorosny
Superconductivity and Advanced Materials Group, School of Engineering, São Paulo State University (UNESP), Campus at Ilha Solteira, Ilha Solteira, Brazil
e-mail: alexsander.pessoa@gmail.com

C. L. Cavalho
e-mail: claudio.carvalho@unesp.br

R. Zadorosny
e-mail: rafazad@gmail.com

A. Koblischka-Veneva · M. R. Koblischka (✉)
Experimental Physics, Saarland University, Saarbrücken, Germany
e-mail: miko@shibaura-it.ac.jp

A. Koblischka-Veneva
e-mail: anjela@shibaura-it.ac.jp

Present Address:
A. Koblischka-Veneva · M. R. Koblischka
Shibaura Institute of Technology, Tokyo, Japan

Introduction

Since the discovery of ceramic superconductors (HTSc), a variety of applications have been proposed (Seeber 1999; Seidel 2015). However, there are still persistent implementation difficulties of the present day HTSc materials, which are related to low transport current densities, high ac-losses, their brittleness, and the high production costs (Bray 2009). For massive, bulk materials required for trapped field applications (Cardwell et al. 2004), the oxygenation processes and the cooling of the samples can also be a problem (Reddy and Schmitz 2002; Haran et al. 2017). Thus, focusing on a more accessible material to be cooled, high-porous superconductors can be good specimens to be studied (Koblischka and Koblischka-Veneva 2018).

In this point of view, superconducting nanowire networks of $YBa_2Cu_3O_{7-\delta}$ (YBCO) were prepared by the solution blow spinning (SBS) technique (Daristotle et al. 2016; da Costa Farias et al. 2015; Cheng et al. 2014). The resulting samples are fabric-like networks or fiber mats of nanowires, being very similar to the nanowire network samples fabricated by electrospinning of YBCO (Duarte et al. 2015) and $Bi_2Sr_2CaCu_2O_{8+\delta}$ (Bi-2212) (Koblischka et al. 2016a; b; Zeng et al. 2017a; b). All these nanofiber mats are nanoporous materials which are characterized by their extremely low weight (the typical density of the samples is only about 0.05 g/cm^3).

The magnetic properties of these nanofiber mat samples have shown already a quite peculiar behavior in previous publications (Koblischka et al. 2016a, b; Zeng et al. 2017a; b). This includes a well-developed granular character of the magnetization loops, a superconducting transition temperature, T_c, which is commonly smaller than that of the bulk counterparts, and the presence of dia- or paramagnetic moments distorting the magnetization loops (MHLs).

In the present contribution, we show that the YBCO nanofiber mats exhibit the paramagnetic Meisser effect (abbreviated PME), but in a distinctly different appearance as compared to previous reports. Several types of high-T_c superconductors have shown the PME (Braunisch et al. 1992; Braunisch et al. 1993; Rice and Sigrist 1995). The samples studied to exhibit the PME were mostly Bi-2212 bulks, while the PME was not observed in tape-like materials of the same chemical composition. The observation of a similar PME in conventional metallic superconductors like Nb (Thompson et al. 1995; Půst et al. 1998; Geim et al. 1998) speaks against explanations like d-wave superconductivity and favors the giant vortex model or flux trapping effects (Koshelev and Larkin 1995; Moshchalkov et al. 1997). All these models for the PME were reviewed in Ref. Li (2003).

In Ref. Koblischka et al. (2000), the PME was observed on an artificially granular YBCO thin film sample. This thin film sample (thickness 150 nm on $SrTiO_3$) was patterned into many disks by electron-beam lithography (diameter 50 μm, contact width 3.5 μm), which were touching each other in order to enable the flow of a transport current through the disks. This type of sample was originally intended to simulate the magnetic behavior of Bi-2212/Bi-2223 tapes, especially concerning the zero-field peak position in the MHL (Koblischka et al. 1997; Koblischka et al. 1999). Additionally, the PME was observed in this sample, but in stark contrast to the bulk Bi-2212 samples (Braunisch et al. 1992; Braunisch et al. 1993) only at very low applied magnetic fields in the μT-range, and when applying larger fields, the $M(T)$-curves recorded were again of the archetypal type. This type of PME was ascribed in Ref. Koblischka et al. (2000) to the field-trapping in the open spaces between the disks. This artificially granular thin film sample enables now a comparison to the present microporous nanofiber mats of the same material (YBCO), and thus, a conclusion of the origin of the PME in the YBCO nanofiber mats can be reached.

Thus, we focus here on details of the sample microstructure and analyze the magnetic properties of the SBS-prepared YBCO nanofiber mats by discussing the current flow in such nanoporous samples in detail.

Experimental procedures

Sample preparation

A one-pot-like chemical route (Rotta et al. 2020) was used to prepare the precursor solution. Yttrium-(III)-acetate hydrate ($C_6H_9O_6 \cdot xH_2O$, 99.9% from Sigma), barium acetate ($C_4H_3BaO_4$, 99%), and copper-(II)-acetate monohydrate ($C_4H_6CuO_4 \cdot H_2O$, 99%) both from Sigma-Aldrich were stoichiometrically dissolved in a ratio Y:1-Ba:2-Cu:3 in a single vessel with 16.6 ml of solution. The used solvents were methanol 59.2 wt%, propionic acid 24 wt%, and acetic acid 16.8 wt%. After 5 min of stirring, polyvinylpyrrolidone (PVP, 1 million 3 hundred thousand g/mol) in a concentration of 5.75 wt% was gradually added in an acetate:PVP weight ratio of 5:1. The precursor solution was stirred for 24 h in a hermetically closed vessel to guarantee its stability, solubility, and homogeneity. Then, the solution was loaded in a 10-ml syringe and spun using the solution blow spinning (SBS) technique as described in Refs. (Rotta et al. 2016; Rotta et al. 2019) with an injection rate of 3 ml/h. The needle

used was of type 25G (0.5-mm diameter) and the air pressure was adjusted to 1 kPa with the collector set to 40 cm, and the rotation speed at 40 rpm.

The green sample (as-collected fibers) was subsequently heat-treated at 100 °C for 1 h and 150 °C for another hour. The subsequent heat treatment was carried out under oxygen flux. The temperature was ramped up at 1 °C/min up to 600 °C and kept there for 3 h, and then, at 3 °C/min to 925 °C and maintained there for 1 h. After that, the temperature was decreased at a rate of −3 °/min to 750 °C and remained there for 6 h. In a final step, the temperature was decreased at −3 °C/min to 450 °C. After 24 h, the gas flow and the oven was turned off, reaching room temperature by furnace thermal inertia. The constituent phase was checked by means of x-ray diffraction (see Fig. 2c), revealing a pure YBCO phase with only minor secondary phases.

Microscopy

The scanning electron microscopy analysis was performed in a JEOL 7000F SEM microscope equipped with a TSL (TexSEM Labs, UT) analysis unit for electron backscatter diffraction (EBSD). TEM investigations were performed using a JEOL JSM-2011 transmission electron microscope (200 kV, LaB_6 cathode). The samples intended for TEM and EBSD were placed on a carbon-coated Cu-TEM grid.

Magnetic measurements

Magnetic measurements were performed using a Quantum Design MPMS3 SQUID system equipped with VSM option. The applied field was ±7 T (field sweep rate 0.36 T/min). Additional measurements were performed with a MPMS-5 SQUID magnetometer including the ultra low-field option.[1] Magnetic fields smaller than 0.5 mT were generated by a Cu coil, which is part of the ultra-low-field option. Scan lengths of 1 cm and 4 cm were employed to test effects of field inhomogeneity; magnetic moments were evaluated directly from the SQUID voltage output.

[1]Quantum Design, San Diego, CA 92121, models MPMS3 and MPMS5S with ultra-low-field option

Results and discussion

Microstructural features

Figure 1a and b present the microstructure of the YBCO nanofiber mat sample. In the low magnification image (a), one can see a fiber mat with several nanowires standing out of the plane. The inset presents a piece of a fully reacted nanofiber mat. Note the large size of such nanofiber mats which can easily reach cm^2 dimensions. The overall nanofiber mat is a nanoporous superconductor, which is revealed in Fig.1b, where one can see the arrangements of the individual nanofibers and the numerous interconnects between them. The samples consist of numerous, relatively long (up to 10 μm) nanowires with an average diameter of ≈ 560 nm, resulting in a non-woven fabric with numerous interconnects between the individual nanowires.

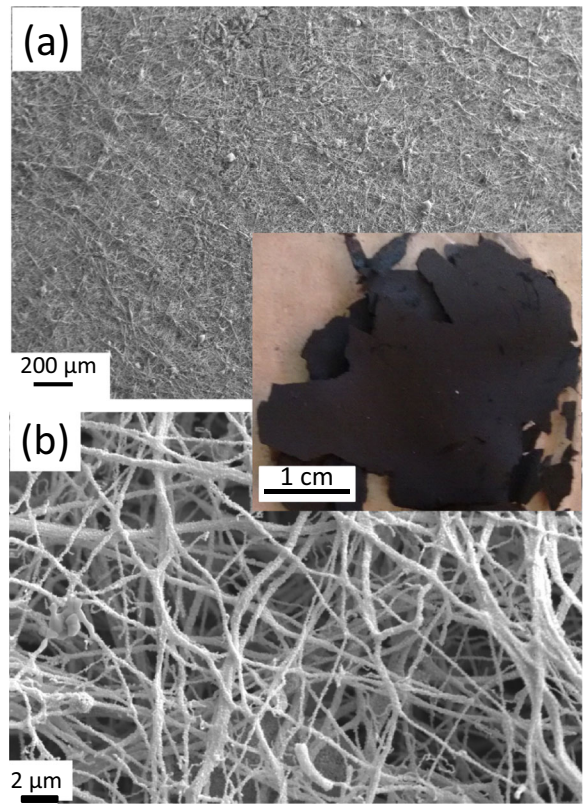

Fig. 1 SEM images of the microstructure of the YBCO nanofiber mats at various magnifications (× 100 (**a**), × 5000 (**b**)). The inset presents a piece of the fully reacted YBCO nanofiber mat in an optical image

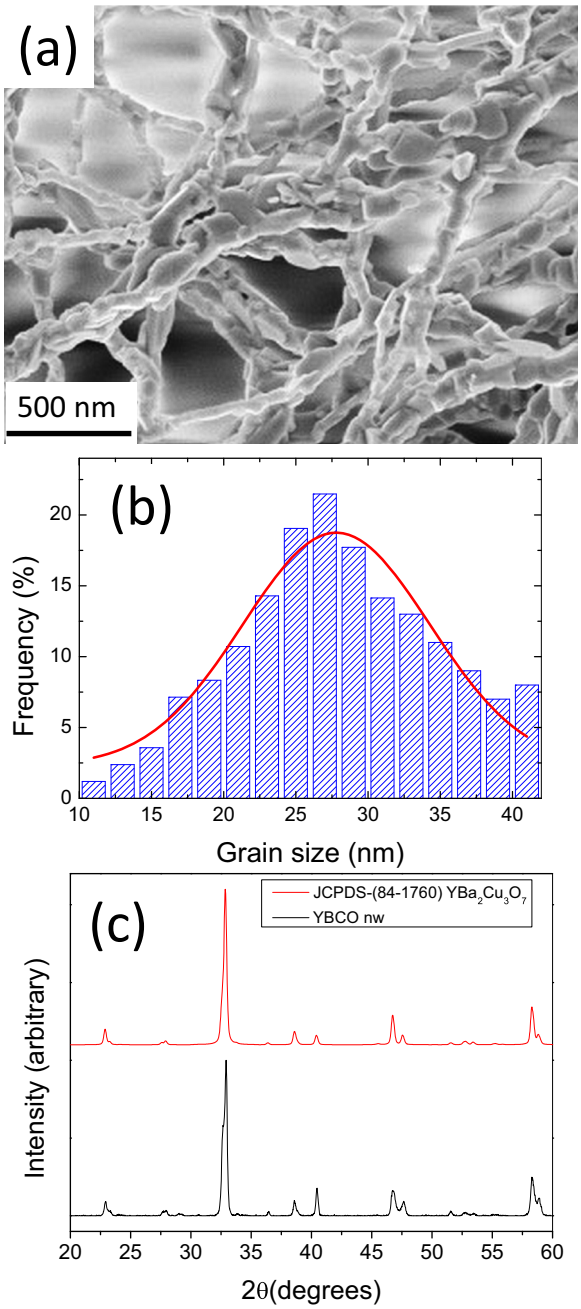

Fig. 2 **a** Low-resolution, bright-field TEM image of the nanowire structure revealing the YBCO grains and the interconnects between the nanowires. **b** Grain size statistics obtained from TEM dark and bright field images. **c** X-ray diffractogram of the YBCO nanofiber mat sample

Figure 2a shows a low-resolution TEM image revealing the arrangement of the YBCO grains. From some fibers, there are YBCO grains sticking out, resulting in a rough surface of the nanowires. An analysis of EBSD was attempted as in Ref. Koblischka-Veneva et al. (2018), but only on some places Kikuchi patterns could be obtained, which is a direct consequence of the surface roughness. The low TEM resolution for this images was chosen to better visualize the numerous interconnects between the nanowires, which are important for the flow of the transport currents in the nanowire fiber mats. Also, such interconnects may comprise more than two nanowires. Furthermore, we can see here that the nanowires themselves are formed by superconducting YBCO grains, which are stacked together. Figure 2b shows the determination of the average grain size by a Gauss fit. The average YBCO grain size is $\sim$ 28 nm as determined from several bright and dark field TEM images to enable the distinction of grains and subgrains. In an extreme case, a single nanowire can be as thin as one single YBCO grain. The fully reacted nanofiber mats are quite brittle, and it is possible to separate individual nanowires by means of focused ion-beam cutting from the remainder of the sample. Figure 2c presents the x-ray diffractogram and the comparison with the JCPDS file for fully oxygenated YBCO. The analysis reveals that the YBCO nanofiber mats are pure YBCO with only some minor secondary phases begin present. More details of the preparation of the YBCO nanowires by SBS and the optimization of their morphology and yield were previously reported in Ref. Rotta et al. (2020).

Magnetization data and PME

In Fig. 3, the $m(H)$-curves of the SBS-YBCO sample are presented. We can see that at low temperatures (4.2 K, 10 K), a superconducting diamagnetic signal is obtained. The entire magnetization loop is, however, overlaid with a paramagnetic contribution. This paramagnetic signal may stem from the copper ions. On increasing the temperature, the diamagnetic contribution is reduced. At $T = 60$ K, the $m(H)$-loop hardly reveals a superconducting contribution, except in the center. All $m(H)$-loops recorded on the nanofiber mats are strongly asymmetric, which is a consequence of the granularity. When comparing these $M(H)$-loops to those of electrospun Bi-2212 nanofiber mats (Koblischka et al. 2016b), one can notice that the granularity/asymmetry is much stronger for the present YBCO nanofiber mats as for the Bi-2212 samples.

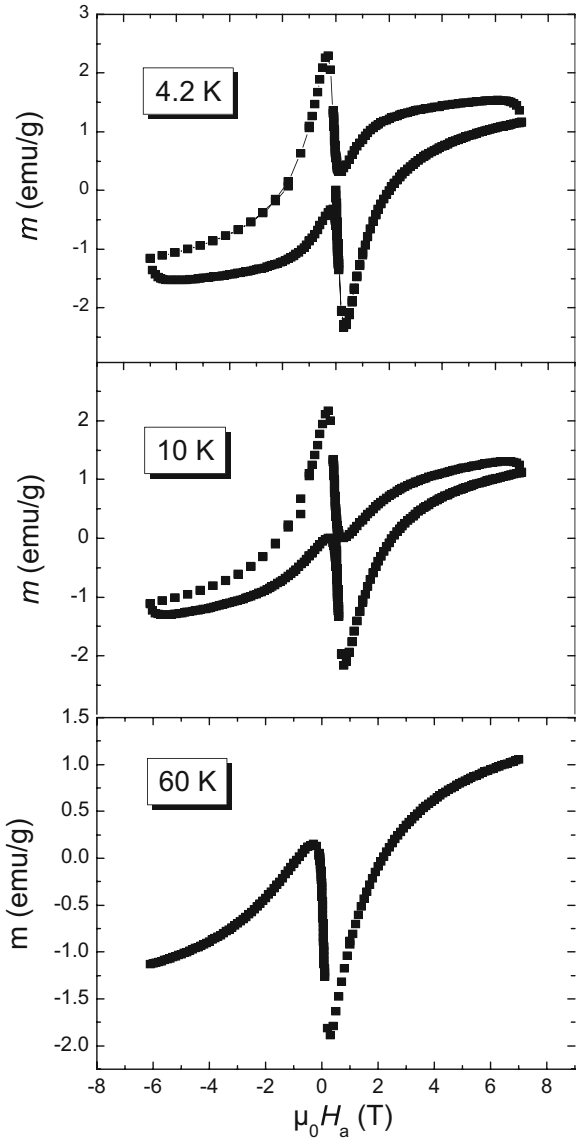

Fig. 3 Magnetization loops measured at $T = 4.2$ K (**a**), 10 K (**b**), and 60 K (**c**). Note the strong granular character of the MHLs (asymmetric shape) and the presence of a paramagnetic moment, which is overlaid on the superconducting signal

Figure 4 presents FCC (field-cool cooling) measurements in two selected applied magnetic fields, which clearly reveal the different behavior of the sample in the μT-range and mT-range fields. The onset of superconductivity in the YBCO nanowire fiber mat is observed at 91 K, which is similar to the bulk counterparts. In applied magnetic fields above 0.5 mT, the $m(T)$ signal stays always negative as it is expected from a superconducting sample, which is in strong contrast to the PME measurements on the bulk Bi-2212 or Nb. At $T < 10$ K (blue dotted circle), there is an evident upturn of the Meissner curve. This upturn of $m(T)$ is again due to the paramagnetic contribution of copper, which is often seen on $m(T)$ curves of YBCO samples (Luzhbin et al. 2004). A paramagnetic Meissner response is observed in applied magnetic fields < 0.35 mT; however, the magnitude of the PME is very small when comparing the magnetic moment with those recorded on the bulk Bi-2212 or Nb samples (see Refs. Braunisch et al. (1993) and Půst et al. (1998)). The inset to Fig. 4 shows a magnification of the PME close to T_c. Here, we must note that $m(T)$ of the PME is always positive right from T_c, which is again contrasting the PME of the bulk Bi-2212 or Nb samples (Braunisch et al. 1993; Půst et al. 1998)), where $m(T)$ starts towards negative values at the onset of superconductivity and then turns towards positve values at a temperature, T^*. This change of direction of $m(T)$ can be observed there on both FCC and FCW curves, whereas in the present case, the FCC and FCW curves practically coincide.

Figure 5a presents more PME measurements in several applied magnetic fields on the YBCO nanofiber mat sample. Reducing the applied magnetic field from 500 to 45 μT creates a much more positive magnetic moment, which saturates at 45 μT. Even smaller fields (we can apply 4.5 μT) cause practically the same curve. These measurements were, however, very noisy, so we omitted them for clarity. Furthermore, Fig. 5a also shows the zero-field cooled $m(T)$-signal (cooling the sample down to 2 K, and then applying the denoted field), which is completely negative without any special feature.

Thus, the PME of the YBCO nanofiber mats may be purely due to flux trapping effects in the open spaces between the nanowires like discussed in Refs. (Koshelev and Larkin 1995; Moshchalkov et al. 1997). Furthermore, the resulting PME is small due to the nanosize of the superconducting current loops involved. Here, we must note that there are currents flowing through the entire sample perimeter (shielding currents), but there are also current loops around the internal pores and current loops in each superconducting YBCO grain (dos Santos et al. 2006). As the grain boundaries (GBs) in YBCO are showing a much more pronounced weak-link character as in the Bi-based superconductors (Hilgenkamp and Mannhart 2002; Hensel et al. 1995), the currents between the

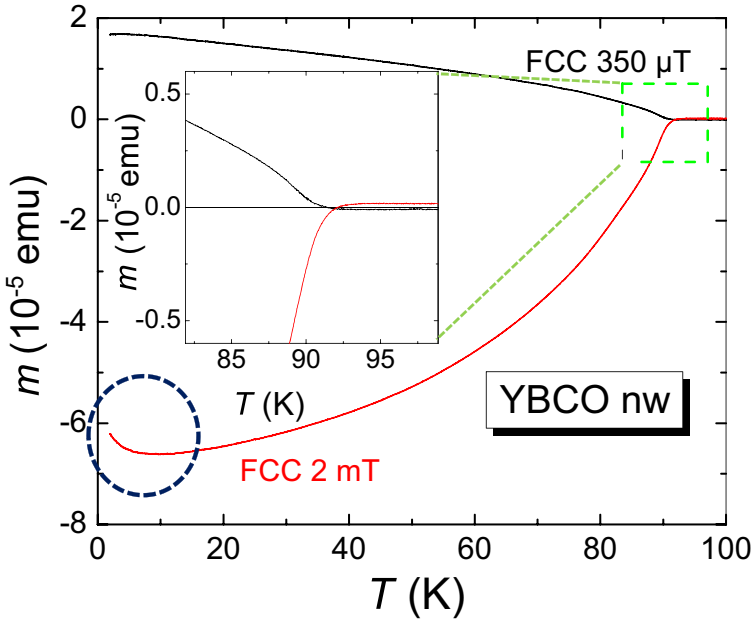

Fig. 4 $m(T)$-behavior of the YBCO nanowire fiber mat when field-cooling the sample in 2 mT applied field (red line) and 350 μT (black line). The inset gives a magnification around T_c. Note here that the PME signal always stays positive

grains and through the interconnects are much smaller as the intragranular currents in the sample.

Now it remains the question why we did not observe a PME in the Bi-2212 nanowire samples studied previously. This may be explained in part regarding the different GB characteristics but is mainly due to the different temperature behavior of the current density of the two materials: In Bi-2212, there is a 3D-2D transition at $\sim$ 50 K (Koblischka and Sosnowski 2005), and as a result, the critical current density is much reduced at elevated temperatures close to T_c as for YBCO, which stays 3D-like up to T_c. This is due to the fact that the intragranular currents in YBCO are much stronger at elevated temperatures as compared to Bi-2212.

To further manifest the origin of the PME in the YBCO nanofiber mat samples, we compare the present data with the PME of the artificially granular YBCO thin film sample, which were published in Ref. Koblischka et al. (2000). The dimensions of this thin film sample are as follows: thickness 150 nm on $SrTiO_3$ substrate, patterned into $\sim$ 8000 disks by electron-beam lithography (diameter of the disks 50 μm, contact width $w = 3.5$ μm). Figure 5a and b show

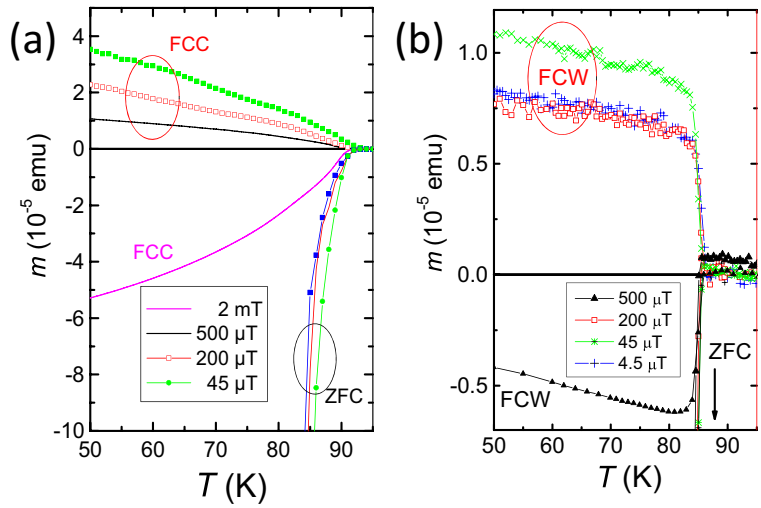

Fig. 5 Comparison of the PME of the YBCO nanofiber mats (**a**) to the artificially granular YBCO thin film sample patterned by electron-beam lithography (**b**). Note the similarity of the PME effect in the two types of samples as in both cases, the PME appears only at very low applied magnetic fields, and above a certain applied field, the FCC curves do exhibit the archetypal shape again

the comparison of the PME data. The magnetic and magneto-optical properties of the artificially granular YBCO thin film sample were discussed in detail in Refs. (Koblischka et al. 1997; Koblischka et al. 1999). There are, however, no weak-links between the YBCO disks, only the current path is confined to the contact width, w.

Both samples exhibit the PME in a remarkably similar way. At low magnetic fields in the μT-range, the paramagnetic signal is strong. Increasing the applied magnetic field leads to a smaller PME, until the PME completely vanishes for fields > 500 μT. All higher applied magnetic fields lead to an archetypal behavior. For the ZFC curves, always a negative signal is obtained. Furthermore, both samples do not exhibit the characteristics of the PME seen on bulk Bi-2212 and Nb: The PME signal is positive right from the onset of superconductivity and does not go slightly negative before turning up towards positive values. All this similarity of the PME leads straightforwardly to the conclusion that the PME in these two types of samples has the same origin.

Finally, Fig. 6a gives a schematic sketch of the current flow in the nanofiber mat. Supercurrents shielding the space in between the individual nanowires and shielding the entire sample perimeter (inter-wire currents) must flow across the interconnects as indicated by — (inter-wire currents, $j_{c,\text{inter-wire}}$). These interconnects are playing a very important role for the superconducting performance of the nanofiber mats, and previous resistance measurements on such samples (Koblischka et al. 2016a) have shown that such currents can flow even in 10 T applied magnetic field, which is hardly possible in standard, polycrystalline samples. Inside a nanowire, the supercurrents can flow inside the YBCO grains (intragranular currents, $j_{c,\text{intra}}$), and along the nanowire length via the grain boundaries (intergranular currents, $j_{c,\text{inter}}$) as depicted in Fig. 6b. According to the results presented in Ref. Koblischka et al. (2016a), we have $j_{c,\text{intra}} > j_{c,\text{inter}} \simeq$

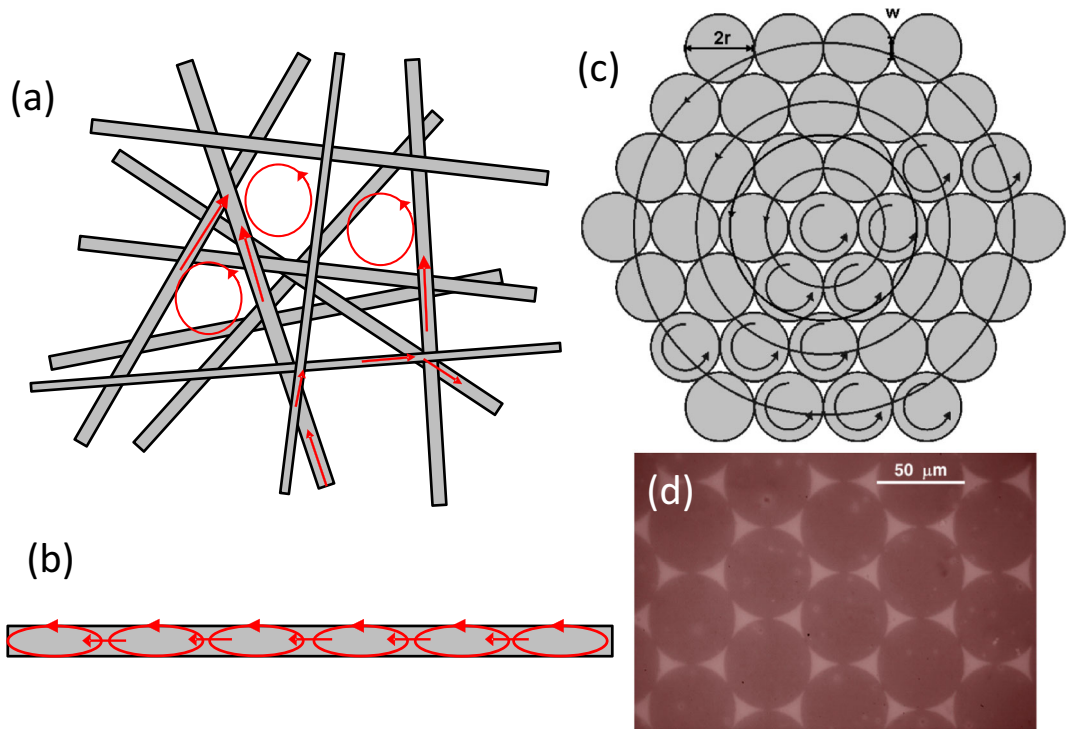

Fig. 6 **a** Schematics of the supercurrent flow of the entire nanofiber mat sample (inter-wire currents), and **b** the current flow *within* an individual nanowire (intergranular and intragranular currents). The current flow is indicated using red arrows (—). **c** The supercurrent flow in the artificially granular YBCO thin film. In (**c**), the layout of the artificially granular thin film sample is sketched. In the upper row of circles, the definition of the contact width, w, is indicated. Finally, in (**d**), a photograph of the realized YBCO thin film sample is presented consisting of about 8000 disks

$j_{c,\text{inter-wire}}$, which reflects the negative influence of the GBs on the supercurrents as well as the positive contribution of the interconnects. These three current contributions (i.e., one more as in a common sintered, polycrystalline sample) describe the current flow in the nanofiber mats.

Figure 6c illustrates the current flow in the artificially granular thin film. The currents can flow within an individual disk, around the entire structure via the contact area w as indicated, and also around the open spaces in between the disks, which can be shielded by small current loops. Thus, the current flow in this special thin film sample is principally similar to that of the nanofiber mats. The characteristics of the first two types of currents were demonstrated in Ref. Koblischka et al. (1999) using magneto-optic imaging. Finally, Fig. 6d gives an optical image of the realized artificially granular thin film sample. Here, we have to note that the superconducting disks are arranged in a single plane, and all the empty spaces between the disks have the same geometry. In contrast, the nanofiber mat is a true 3D arrangement of the nanowires, and the voids between the nanowires are fully irregular. These features and the very strong currents of an epitaxial YBCO thin film are responsible that the magnitude of $m(T)$ of both sample types is similar, even though there is less superconducting material in the thin film sample. Both sample types have in common that the currents can shield the open spaces in the structure. Thus, we may conclude here that the trapping of flux in these spaces is responsible for this type of PME.

Conclusion

We have presented magnetization data of YBCO nanofiber mats prepared by the solution blow spinning technique. The $m(H)$-curves reveal strong granularity and an onset of superconductivity at 91 K. Performing field-cooling in small applied magnetic fields in the μ-T range, the YBCO nanofiber mats reveal the PME, but the properties of the PME are similar to that of an artificially granular YBCO thin film sample, and not to bulk Bi-2212 or Nb. This points to a PME being entirely due to flux trapping in the spaces in between the nanowires.

Acknowledgments We acknowledge the assistance of Q. Nouailhetas (GREEN, University of Lorraine, Nancy, France) and C. Chang, T. Hauet (IJL Nancy, France) in some of the magnetic measurements.

Funding Open Access funding enabled and organized by Projekt DEAL. This work is part of the SUPERFOAM international project funded by ANR and DFG under the references ANR-17-CE05-0030 and DFG-ANR Ko2323-10, respectively. ALP and RZ thank the Brazilian agencies São Paulo Research Foundation (FAPESP, Grant 2016/12390-6), Coordenação de Aperfeiçoamento de Pessoal de Nível Superior - Brasil (CAPES) - Finance Code 001, and National Council of Scientific and Technological Development (CNPq, grant 302564/2018-7).

Compliance with ethical standards

Conflict of interest The authors declare that they have no conflict of interest.

References

Braunisch W, Knauf N, Bauer G, Kock A, Becker A, Freitag B, Grütz R., Kataev V, Neuhausen S, Roden B, Khomskii D, Wohlleben D, Bock J, Preisler E (1993) Paramagnetic Meissner effect in high-t_c superconductors. Phys Rev B 48:4030–4042. https://doi.org/10.1103/PhysRevB.48.4030

Braunisch W, Knauf N, Kataev V, Neuhausen S, Grütz A., Kock A, Roden B, Khomskii D, Wohlleben D (1992) Paramagnetic Meissner effect in Bi high-temperature superconductors. Phys Rev Lett 68:1908–1911. https://doi.org/10.1103/PhysRevLett.68.1908

Bray JW (2009) Superconductors in pplications: Some practical aspects. IEEE Trans Appl Supercond 19:2533–2539. https://doi.org/10.1109/TASC.2009.2019287

Cardwell DA, Murakami M, Zeisberger M, Gawalek W, Gonzallez-Arrabal R, Eisterer M, Weber HW, Fuchs G, Krabbes G, Leenders A, Freyhardt HC, Chaud X, Tournier R, Hari Babu N (2004) Round robin measurements of

the flux trapping properties of melt-processed Sm-Ba-Cu-O bulk superconductors. Physica C 412-414:623–632. https://doi.org/10.1016/j.physc.2004.01.082

Cheng B, Tao X, Shi L, Yan G, Zhuang X (2014) Fabrication of ZrO_2 ceramic fiber mats by solution blowing process. Ceram Int 40:15013–15018. https://doi.org/10.1016/j.ceramint.2014.06.104

da Costa Farias RM, Menezes RR, Oliveira JE, de Medeiros ES (2015) Production of submicrometric fibers of mullite by solution blow spinning (SBS). Mater Lett 149:47–49. https://doi.org/10.1016/j.matlet.2015.02.111

Daristotle JL, Behrens AM, Sandler AD, Kofinas P (2016) A review of the fundamental principles and applications of solution blow spinning. ACS Appl Mater Interf 8:34951–34963. https://doi.org/10.1021/acsami.6b12994

dos Santos CAM, Oliveira CJV, da Luz MS, Bortolozo AD, Sandim MJR, Machado AJS (2006) Two-fluid model for transport properties of granular superconductors. Phys Rev B 74:184526. https://doi.org/10.1103/PhysRevB.74.184526

Duarte EA, Rudawski NG, Quintero PA, Meisel MW, Nino JC (2015) Electrospinning of superconducting YBCO nanowires. Supercond Sci Technol 28:015006. https://doi.org/10.1088/0953-2048/28/1/015006

Geim AK, Dubonos SV, Lok JGS, Henini M, Maan JC (1998) Paramagnetic Meissner effect in small superconductors. Nature 396:144–146. https://doi.org/10.1038/24110

Haran KS, Kalsi S, Arndt T, Karmaker H, Badcock R, Buckley B, Haugan T, Izumi M, Loder D, Bray JW, Masson P, Stautner EW (2017) High power density superconducting rotating machines-development status and technology roadmap. Supercond Sci Technol 30:123002. https://doi.org/10.1088/1361-6668/aa833e

Hensel B, Grasso G, Flükiger R (1995) Aspects of the current understanding of the supercurrent transport in $(Bi,Pb)_2Sr_2Ca_2Cu_3O_{10}$ silver sheathed tapes - The railway switch model. J Electron Mater 24:1877-1881. https://doi.org/10.1007/BF02653002

Hilgenkamp H, Mannhart J (2002) Grain boundaries in high-T_c superconductors. Rev Mod Phys 74:485–549. https://doi.org/10.1103/RevModPhys.74.485

Koblischka MR, Koblischka-Veneva A (2018) Porous high-t_c superconductors and their applications. AIMS Mater Sci 5:1199–1213. https://doi.org/10.3934/matersci.2018.6.1199

Koblischka MR, Půst L, Chikumoto N, Murakami M, Nilsson B, Claeson T (2000) Paramagnetic Meissner response of an artificially granular YBCO thin film. Physica B 284-288:599–600. https://doi.org/10.1016/S0921-4526(99)02226-7

Koblischka MR, Půst L, Galkin A, Nálevka P (1997) Anomaluos position of the maximum in magnetic hysteresis loops measured on $(Bi,Pb)_2Sr_2Ca_2Cu_3O_{10}$/Ag tapes. Appl Phys Lett 70:514–516. https://doi.org/10.1063/1.119069

Koblischka MR, Půst L, Galkin A, Nálevka P, Jirsa M, Johansen TH, Bratsberg H, Nilsson B, Claeson T (1999) Flux penetration into an artificially granular high-T_c superconductor. Phys Rev B 59:12114–12120. https://doi.org/10.1103/PhysRevB.59.12114

Koblischka MR, Sosnowski J (2005) Temperature-dependent scaling of pinning force data in Bi-based high-T_c superconductors. Eur Phys J B 44:277–280. https://doi.org/10.1140/epjb/e2005-00126-3

Koblischka MR, Zeng XL, Karwoth T, Hauet T, Hartmann U (2016a) Transport and magnetic measurements on $Bi_2Sr_2CaCu_2O_8$ nanowire networks prepared via electrospinning. IEEE Trans Appl Supercond 26:1800605. https://doi.org/10.1109/TASC.2016.254139

Koblischka MR, Zeng XL, Karwoth T, Hauet T, Hartmann U (2016b) Magnetic properties of electrospun nonwoven superconducting fabrics. AIP Adv 6:035115. https://doi.org/10.1063/1.4944747

Koblischka-Veneva A, Koblischka MR, Zeng XL, Schmauch J, Hartmann U (2018) TEM and electron-backscatter analysis (EBSD) on superconducting nanowires. J Phys Conf Ser 1054:012005. https://doi.org/10.1088/1742-6596/1054/1/012005

Koshelev AE, Larkin AI (1995) Paramagnetic moment in field-cooled superconducting plates: Paramagnetic Meissner effect. Phys Rev B 52:13559–13562. https://doi.org/10.1103/PhysRevB.52.13559

Li MS (2003) Paramagnetic Meissner effect and related dynamical phenomena. Phys Rep 376:133–223. https://doi.org/10.1016/S0370-1573(02)00635-X

Luzhbin DA, Pan AV, Komashko VA, Flis VS, Pan VM, Dou SX, Esquinazi P (2004) Origin of paramagnetic magnetization in field-cooled $YBa_2Cu_3O_{7-\delta}$ films. Phys Rev B 69:024506. https://doi.org/10.1103/PhysRevB.69.024506

Moshchalkov VV, Qiu XG, Bruyndoncx V (1997) Paramagnetic Meissner effect from the self-consistent solution of the Ginzburg-Landau equations. Phys Rev B 55:11793–11801. https://doi.org/10.1103/PhysRevB.55.11793

Půst L, Wenger LE, Koblischka MR (1998) Detailed investigation of the superconducting transition of niobium disks exhibiting the paramagnetic Meissner effect. Phys Rev B 58:14191–14194. https://doi.org/10.1103/PhysRevB.58.14191

Reddy ES, Schmitz GJ (2002) Superconducting foams. Am Ceram Soc Bull 81:35–37

Rice TM, Sigrist M (1995) Unusual paramagnetic phenomena in granular high-temperature superconductors—a consequence of d-wave pairing. Rev Mod Phys 67:503–513. https://doi.org/10.1103/RevModPhys.67.503

Rotta M, Motta M, Pessoa AL, Carvalho CL, Deimling CV, Lisboa-Filho PN, Ortiz WA, Zadorosny R (2020) One-pot-like facile synthesis of $YBa_2Cu_3O_{7-\delta}$ superconducting ceramic: Using PVP to obtain a precursor solution in two steps. Mater Chem Phys 243:122607. https://doi.org/10.1016/j.matchemphys.2019.122607

Rotta M, Motta M, Pessoa AL, Carvalho CL, Ortiz WA, Zadorosny R (2019) Solution blow spinning control of morphology and production rate of complex superconducting $YBa_2Cu_3O_{7-x}$. J Mat Sci Mater Electron 30:9045–9050. https://doi.org/10.1007/s10854-019-01236-w

Rotta M, Zadorosny L, Carvalho CL, Malmonge JA, Malmonge LF, Zadorosny R (2016) YBCO Ceramic nanofibers obtained by the new technique of solution blow spinning. Ceram Int 42:16230–16234. https://doi.org/10.1016/j.ceramint.2016.07.152

Seeber B (ed) (1999) Handbook of Applied Superconductivity. IOP Publishing, Bristol

Seidel P (ed) (2015) Applied Superconductivity. Wiley-VCH, Weinheim

Thompson DJ, Minhaj MSM, Wenger LE, Chen JT (1995) Observation of paramagnetic meissner effect in niobium disks. Phys Rev Lett 75:529–532. https://doi.org/10.1103/PhysRevLett.75.529

Zeng XL, Karwoth T, Koblischka MR, Hartmann U, Gokhfeld D, Chang C, Hauet T (2017a) Analysis of magnetization loops of electrospun nonwoven superconducting fabrics. Phys Rev Mater 1:044802. https://doi.org/10.1103/PhysRevMaterials.1.044802

Zeng XL, Koblischka MR, Karwoth T, Hauet T, Hartmann U (2017b) Preparation of granular Bi-2212 nanowires by electrospinning. Supercond Sci Technol 30:035014. https://doi.org/10.1088/1361-6668/aa544a